Available online at www.sciencedirect.com
ScienceDirect
Journal of Power Sources 171 (2007) 870–878
JOURNAL OF POWER SOURCES
www.elsevier.com/locate/jpowsour

Electrochemical properties of electrodeposited nicked phosphide thin films in lithium cells

Manuel Cruz [a], Julián Morales [a], Luis Sánchez [a,*], Jesús Santos-Peña [a,*], Francisco Martín [b]

[a] *Departamento de Química Inorgánica e Ingeniería Química, Facultad de Ciencias, Campus de Rabanales, Edificio Marie Curie, Universidad de Córdoba, 14071 Córdoba, Spain*
[b] *Laboratorio de Materiales y Superficie (Unidad Asociada al CSIC), Universidad de Málaga, Spain*

Received 28 July 2006; received in revised form 13 June 2007; accepted 2 July 2007
Available online 17 July 2007

Abstract

Thin films of Ni_3P *ca.* 400 nm in thickness were obtained by electrodeposition on a stainless steel substrate and subsequent heating at 500 °C in an argon or vacuum atmosphere. The films were found to consist of *pseudo*-spherical agglomerates of nanosized particles (less than 70 nm in size). Both types of atmospheres induced the formation of coating layers composed of metal oxide species (particularly iron oxide) by effect of the presence of oxygen traces in the environment. As revealed by the XPS depth profile analysis, the layers were thicker when heating under argon. Film thickness determined the electrochemical reactivity towards lithium. Oxide and electrolyte reduction were the main electrochemical reactions undergone by the film on discharging the cell, the Ni–P alloy component being scarcely affected. Based on XRD, XPS and electrochemical measurements, the pristine film heated under vacuum also reacted partially with lithium to give nickel and lithium phosphide. However, the reversibility of this reaction is limited and the capacity delivered by the resulting cells was low (lower than that calculated from the reaction stoichiometry, but significantly higher than that obtained from the electrode made from the bulk alloy).

Keywords: Nickel phosphide; Negative electrode; Lithium ion batteries; Electrodeposition; Pnictides

1. Introduction

Much of the interest of researchers in lithium ion batteries has so far focussed on developing negative electrodes with properties comparable to or even better than those of graphite. 3D transition metal oxides, M_xO_y, have recently been proposed as alternative anode materials [1]. M_xO_y systems exhibit low irreversibility in the electrochemical reaction and scarce mechanical failure; also, they provide specific capacity values as high as 700 A h kg^{-1} on extended cycling [2–6]. Their excellent electrochemical performance is the result of a simple, yet highly reversible reaction with lithium ions: $M_xO_y + 2y\ Li^+ + 2y\ e^- \Leftrightarrow x\ M + y\ Li_2O$.

This finding has promoted research into various other transition metal derivatives including fluorides [7], nitrides [8] and pnictides [9]. Despite their interesting electrochemical properties, the practical use of oxides and fluorides in lithium batteries is dubious owing to their wide working potential window (3.0–0.0 V). Therefore, current research is focussing on transition metal compounds capable of reacting with lithium at lower potential values (1.5–0.0 V).

In this context, some phosphides have the ability to react with Li over a narrow potential range (a low charge–discharge polarization, $\Delta V \approx 0.4$) at an average potential of 1.0 V versus Li^+/Li. These electrochemical characteristics are interesting with a view to developing new negative electrodes. Some studies on M_xP_y (M = Mn, Fe, Co, Cu) [9–12] and $Li_zM_xP_y$ [13,14] phosphides have shown the reversibility of the electrochemical reaction and its underlying mechanism to depend on the particular crystal structure, as well as on the M/P and Li/P ratios in the starting compound. However, the cycling performance of these electrode materials has been deemed poor and some attempts at enhancing their cyclability have been made with Cu_3P [15] and NiP_2 [16] systems. The particular method used to prepare these compounds

* Corresponding authors. Tel.: +34 957 218620; fax: +34 957 218621.
E-mail addresses: luis-sanchez@uco.es (L. Sánchez), iq2sanpe@uco.es (J. Santos-Peña).

0378-7753/$ – see front matter © 2007 Elsevier B.V. All rights reserved.
doi:10.1016/j.jpowsour.2007.07.013

as metallic films and changes in particle size have been identified as two key factors governing their cycling performance.

Based on previous work of our group on anode materials, electrodes prepared as thin films usually exhibit a long cycle life [5,6]. Also, we have found electrodeposition to be an excellent method for preparing thin films of anode materials. Moreover, electrodeposition is a simple, low-cost method for preparing nickel–phosphorus alloys [17–20] used as protective coatings against corrosion. In this work, electrodeposited amorphous Ni–P alloy was prepared as thin films in a typical bath containing nickel salts and sodium hypophosphite. Crystallization was accomplished in two different atmospheres (*viz*. vacuum and argon) and provided the phase Ni_3P. The physico-chemical characterization of the different films and the examination of their electrochemical properties as electrode materials for lithium batteries were two additional purposes of this work.

2. Experimental

Ni–P alloy deposits were obtained by electrodeposition from solutions with the following composition: $NiSO_4{\cdot}6H_2O$ (174 g L^{-1}), $NiCl_2{\cdot}6H_2O$ (47 g L^{-1}), H_3PO_4 (51 g L^{-1}) and $NaH_2PO_2{\cdot}H_2O$ (63 g L^{-1}) [17]. Solutions were prepared from *Panreac* analytical grade chemicals and MilliQ water. For comparison, electrodeposited nickel was prepared from a conventional Watt's bath as reported elsewhere [21], and so was crystalline Ni_3P by a chemical reduction of the Watt's bath with sodium boronhydride.

Ni–P films were electrodeposited in the galvanostatic mode on stainless steel substrates (Plates 2 cm^2 in surface area). A platinum foil was used as counter-electrode. Prior to electrodeposition, both electrodes were cleaned with acetone. The solution was heated at 80 °C and adjusted to pH 2 by addition of sodium carbonate. Electrodeposition was done, under continuous mild stirring, by passing a current density of 120 mA cm^2 for 20 s. The current was controlled via a Multichannel Arbin BT2000 device. The deposits thus obtained were removed from the solution, thoroughly rinsed with water and air-dried for subsequent heating at 500 °C in an argon or vacuum (5×10^{-2} Torr) atmosphere for 1 h and storage in a glove-box. The electrodeposited nickel film was heated at 500 °C in argon.

X-ray diffraction (XRD) patterns were recorded on a Siemens D5000 X-ray diffractometer, using CuK_α radiation ($\lambda = 1.54059$ Å) and a graphite monochromator. The particle size and morphology of the films were studied with a scanning electron microscope (SEM, JEOL JMS-6400) with an energy dispersive X-rays EDX analyser coupled. X-ray photoelectron spectra (XPS) were recorded on a Physical Electronics PHI 5700 spectrometer using non-monochromated MgKα radiation ($h\nu = 1253.6$ eV), with the X-ray generator operating at 15 kV and 20 mA. Binding energies were corrected with the binding energy values for C(1s) of adventitious carbon fixed at 284.8 eV. Survey spectra over the range 0–1100 eV were recorded at a 187.85 pass energy, each region being scanned several times to ensure an adequate signal-to-noise ratio. A 3×3 mm sample area was sputtered with 4 keV Ar^+; the sputter rate was assumed to be ~4.5 nm min^{-1} as determined for Ta_2O_5 under identical sputtering conditions. Spectra were processed by using PHI-Access V6 and Multipak software, both from Physical Electronics. High-resolution spectra were fitted after Shirley background correction.

Electrochemical measurements were made in a two-electrode cell, using lithium as counter-electrode. The electrolyte used was Merck battery electrolyte LP 40, which consists of 1 M $LiPF_6$ in ethylene carbonate (EC) and dimethyl carbonate (DMC) in a 1:1 w/w ratio. Square 6 mm × 6 mm pieces of stainless steel coated with the active material were used as working electrodes. The amount of active material attached to the substrate was determined by weighing the substrate before and after electrodeposition on a Sartorius microbalance sensitive to within ±1 μg. For *ex situ* XPS, the cells were opened in the glove-box and the electrodes washed with dimethylcarbonate to remove the electrolyte, dried in an inert atmosphere and stored in tightly sealed glass containers under an argon atmosphere for transportation. The containers were opened in a laboratory-made glove box connected to the preparation chamber of the XPS spectrometer. In this way, exposure of the electrodes to air between opening of the cells and transfer of the pellets to the XPS chamber was avoided. A similar procedure was followed for *ex situ* XRD measurements. In this case, inside the glove-box the deposit was covered with a plastic film to avoid contact with air. Cells were galvanostatically charged and discharged at a cycling rate of C/10, C being defined as 3 Li^+ exchanged in 1 h. Step potential electrochemical spectroscopy curves (SPES) were recorded at 100 mV h^{-1} per step in the potential window 3.0–0.0 V. All electrochemical measurements were controlled via a MacPile II potentiostat–galvanostat.

3. Results and discussion

3.1. Physico-chemical characterization of films

As revealed by its XRD pattern, which contained peaks for the stainless-steel substrate alone (Fig. 1a), the Ni–P material

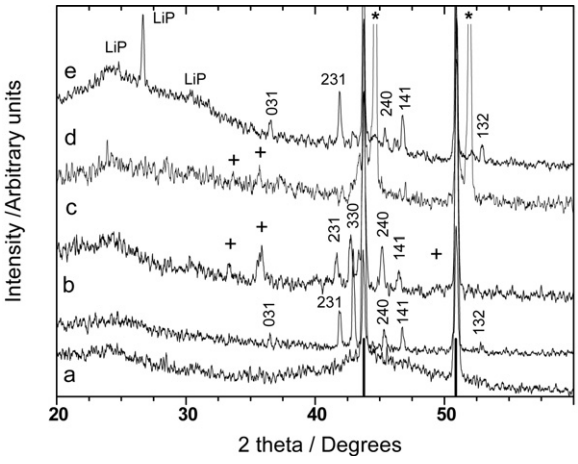

Fig. 1. XRD patterns for Ni–P electrodeposited films: (a) pristine; (b) and (c) heated at 500 °C under vacuum and argon, respectively. (d) Electrodeposited Ni heated at 500 °C under argon and (e) film b upon discharge at 0.0 V. (|) stainless steel, (+) hematite, (*) Ni metal.

obtained by electrodeposition was amorphous. After heating the deposit at 500 °C under argon or vacuum, a set of peaks appeared that was assigned to the Ni_3P compound (ICDD Card No. 34-501) (Fig. 1b and c). In both cases, the intensity ratio between the (2 3 1) and (3 3 0) reflections was different from that for bulk Ni_3P, where the (2 3 1) reflection was the strongest. This indicates a clear tendency for particles to grow along the [*h k 0*] direction. Additionally, the sample heated under argon exhibited weak peaks that can be assigned to the (1 0 4), (1 1 0) and (0 2 4) reflections of hematite Fe_2O_3 (ICDD Card No. 33–664), and reveal that the substrate was partially oxidized under these conditions by effect of the presence of oxygen traces in the carrier gas or the film pores. No peaks for crystallised nickel were observed. On the other hand, the presence of hematite was apparent from the XRD pattern for a nickel electrodeposited film heated under argon (Fig. 1d).

The morphological characteristics of the films are illustrated in Fig. 2. The thickness of the electrodeposited films was rather homogeneous (about 400 nm thick as shown by the cross-sectional view Fig. 2a). In general, the film surface was quite compact and smooth as revealed the top view image shown in Fig. 2b. However, some porous regions were observed at higher magnification, formed by *pseudo*-spherical agglomerates of two different sizes (Fig. 2c). That agglomerates consisting

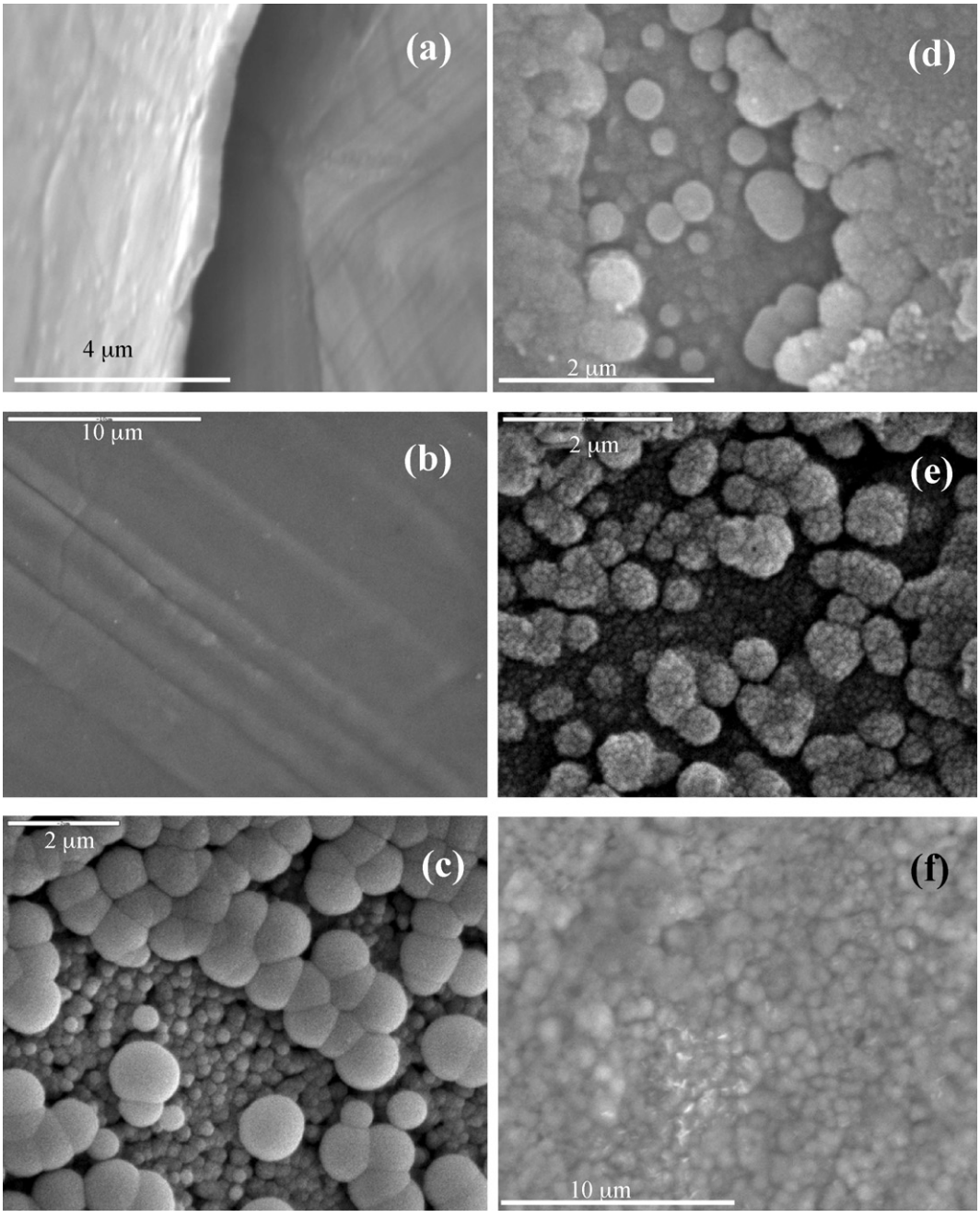

Fig. 2. Cross-sectional and top view SEM images for Ni–P films as deposited (a–c) and after heating at 500 °C for 1 h under vacuum (d) or argon (e). (f) Image of the electrodeposited Ni film.

Table 1
Binding energies (eV) for the emission peaks in the XPS spectra for Ni–P films

Emission peak	Film					
	Original		Heated under vacuum		Heated under argon	
	0*	4	0	16	0	25
	B.E.		B.E.		B.E.	
Fe $2p_{3/2}$	–	–	710.0 (Fe^{III}–O)	–	711.0 (Fe^{III}–O)	–
O 1s	531.9 ($O^{=}$)	–	529.9 ($O^{=}$)	–	531.5 ($O^{=}$)	–
Ni $2p_{3/2}$	856.2 (Ni^{II}–O)	852.6 (Ni_xP)	856.0 (Ni^{II}–O)	852.5 (Ni_xP)	856.4 (Ni^{II}–O)	852.8 (Ni_xP)
P 2p	133.1 ($PO_4^{\equiv}$)	130.1 (Ni_xP)	–	129.4 (Ni_xP)	–	130.2 (Ni_xP)

Assignations are shown in brackets.
* Sputtering time (min).

of the larger particles (*ca.* 1 μm in diameter) exhibited a low density packing. Underneath, a more tightly packed array of particles around 200 nm in diameter was observed. Film morphology changed with the heating atmosphere. The surface of the film heated under vacuum (Fig. 2d) was quite similar to that of the pristine film. Under argon, the surface of the *pseudo*-spherical agglomerates was granulated and suggested the involvement of tiny particles forming a still more porous structure (Fig. 2e). In both cases, the loading of the films was 0.35 mg cm^{-2}. The oxidation reaction undergone by the films could be a plausible explanation for the increased surface roughness. Fig. 2f shows a SEM image of electrodeposited nickel consistent with previously reported findings [21]. The surface contains uniformly distributed submicrometric nickel grains. These deposits are thicker (*ca.* 0.7 μm) and exhibit an increased loading (1.1 mg cm^{-2}).

XPS measurements provided supplementary information towards the structural characterization of the films. The binding energies of the different peaks in the spectra for the pristine and thermally treated films are shown in Table 1. The presence in the heated films of Fe – which was identified by XRD as an oxide in the film heated under argon (see Fig. 1c) – and, more surprising, the absence of P, suggest that the films are coated by a contamination layer the thickness of which was estimated from the XPS depth profiles. The variation of the atomic contents in the different elements studied is shown in Fig. 3. The element C was excluded because it arose from contamination and disappeared within the first minute of etching. No peaks for Fe were detected in the pristine film, which suggests that the substrate surface was thoroughly coated during electrodeposition, as confirmed by the SEM images. Oxygen was detected, but its content dropped on sputtering (Fig. 3a). The fact that P content decreased slowly whereas that of Ni increased abruptly on sputtering suggests that oxygen is bound mainly to Ni. However, the layer thickness is small (less than 10 nm). The two heated films (Fig. 3b and c) exhibited similar Fe contents (*ca.* 6%). However, the time needed for its disappearance was somewhat different (approximately 6 and 12 min under vacuum and argon, respectively). Also, oxygen took a longer time nearly twice to disappear from the latter film, which is suggestive of a thicker coating layer.

The BE of the P 2p peak (133.1 eV, Table 1) is consistent with the presence of phosphate groups at the surface of the pristine film [22]. Upon sputtering with Ar, the peak shifted to lower BE values (129–130 eV) consistent with those reported for Ni–P

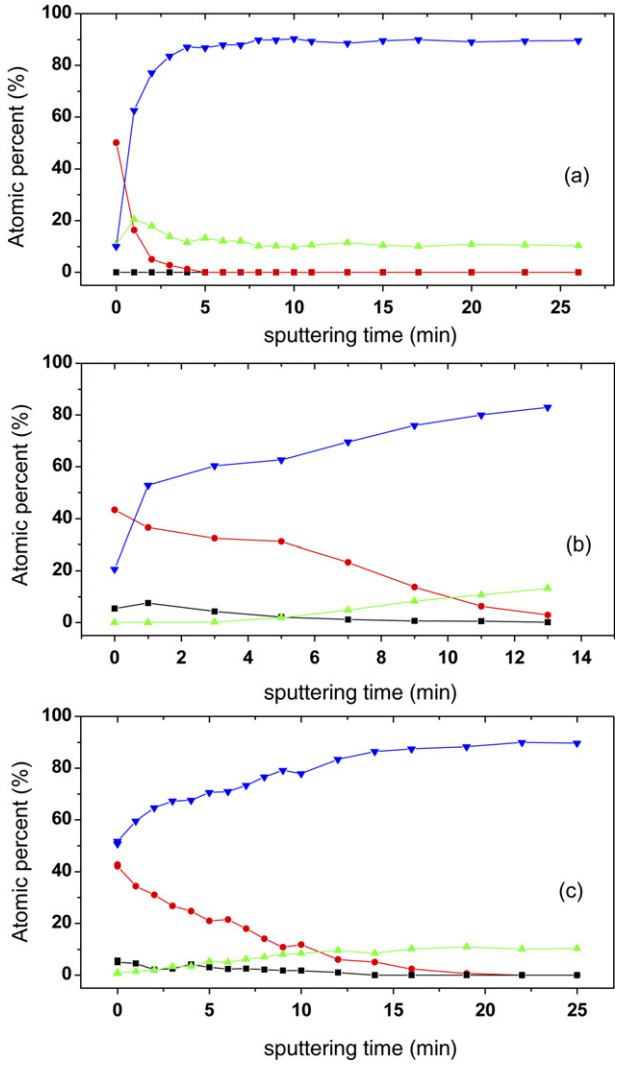

Fig. 3. XPS depth profiles for Ni–P electrodeposited films: (a) pristine; (b) and (c) heated under vacuum and argon, respectively.(▼) Ni, (▲) P, (■) Fe and (●) ○.

compounds [23,24]. Similar BE values were also obtained for the thermally treated films once their presence was detected after few minutes of Ar etching (see Table 1, and Fig. 3b and c). Their content levelled off at around 10% upon prolonged etching.

The calculated BE value for the Ni $2p_{3/2}$ photoemission peak was the same for the three films (856.2 eV) and close to that for Ni bound to oxygen [25]. Upon sputtering with Ar, the peak was also shifted to lower BE levels (852.7 eV, which is close the value for Ni–P compounds [24]). Their content increased with the sputtering time and levelled off at *ca.* 90% after which Ni and P were the sole elements detected in the XPS spectrum (Fig. 3).

The previous results demonstrate that under the experimental conditions used, the electrodeposition process leads to the formation of a Ni-rich phosphide coated with a layer a few nanometers thick of a Ni-based oxide and phosphate. The composition of this layer becomes increasingly complex upon heating, which introduces oxidized Fe from the substrate. Cleaning the surface was more laborious for the heated films (especially those heated under argon) and required prolonged sputtering to remove the contamination layer. We have no convincing explanation for the high Ni/P ratio observed irrespective of the heating treatment used. A higher rate for P sputtering cannot be excluded, but requires confirmation. A Ni/P ratio of 2.55 was obtained from the EDX analysis which is closer to the stoichiometry of the phase detected by XRD. Differences in fundamental principles and the escape depth of the photon emitted from the atom in the two spectroscopic techniques might be the origin of the discrepancy.

3.2. Electrochemical properties of the films in lithium cells

Fig. 4 shows the first two galvanostatic discharge–charge curves for the cells made from the amorphous and crystalline films. The curves were recorded at C/10 and illustrate the variation of the cell voltage with its capacity per gram of electrodeposited material. The shape of the first discharge curve for the electrodes made from the pristine film and that heated under vacuum was quite similar. The voltage continuously faded up to *ca.* 0.8 V, where a very short plateau is observed. Then, the voltage steadily dropped to 0.0 V. The capacity delivered by the two electrodes was similar (around 260 A h kg^{-1}, which is equivalent to the uptake of *ca.* 2 mol of lithium per mol of Ni_3P). The reaction products of the crystalline film were identified from the XRD pattern for the discharged electrode. The pattern (Fig. 1e) contains peaks assigned to nickel and LiP, and others for unreacted Ni_3P. The following reaction is consistent with the presence of these phases:

$$Ni_3P + (1-x)Li \rightarrow (3-3x)Ni + (1-x)LiP + x\text{“}Ni_3P''_{unreacted} \quad (1)$$

However, the calculated capacity at $x=0$ is 130 A h kg^{-1}, which is roughly one-half the experimental value. For many metal phosphides [11–16], the mechanism of the electrochemical reaction with lithium involves the decomposition of the phosphide to give the metal and Li_3P. The lithium phosphide, which is not always detected by XRD, may be formed as an amorphous phase according to the reaction

$$Ni_3P + (3-3y)Li \rightarrow (3-3y)Ni + (1-y)Li_3P + y\text{“}Ni_3P''_{unreacted} \quad (2)$$

The calculated capacity for this reaction should be three times that of reaction (1). On charging, the cells were strongly polarized and the reaction was seemingly poorly reversible (Fig. 4b). In fact, only 75 A h kg^{-1} was recovered on charging. As discussed below, the values obtained on further cycling were similar to this.

The shape of the first discharge curve for the electrode made from the film heated under argon was quite different (Fig. 4c). Thus, a pronounced potential drop from 2.8 to 0.8 V was observed, followed by a broad plateau that accounted for more than one half of the total capacity delivered by the cell. In the last stage, the potential gradually decreased to 0.0 V. Similar profiles have been reported for other transition metal phosphides and oxides used as electrode materials in lithium cells [1,10–12,16,25]. The capacity delivered by the electrode was around 375 A h kg^{-1}, which is close to that calculated from reaction (2) with $y=0$. However, the XRD pattern for the discharged electrode was somewhat unusual, as it only contained

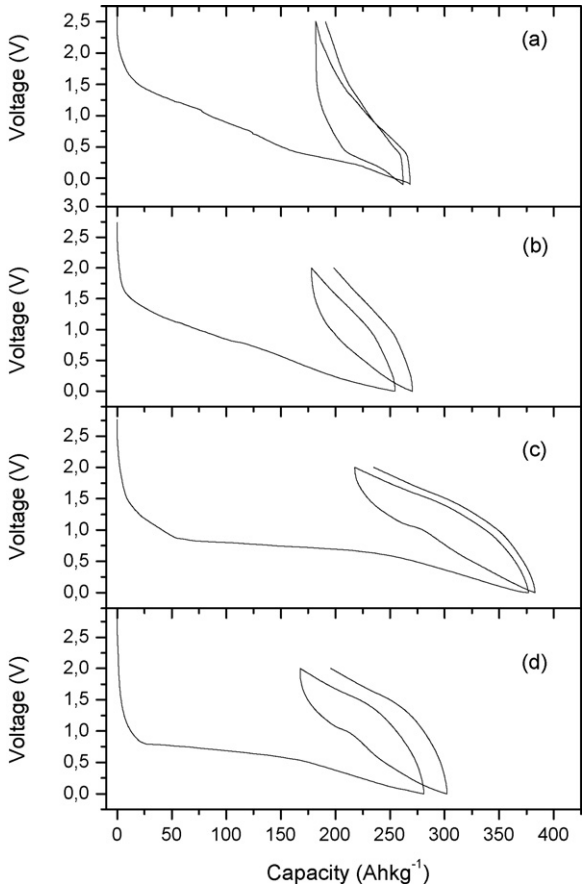

Fig. 4. Galvanostatic curves for Li/electrodeposited Ni–P film cells: (a) pristine film; (b and c) films heated under vacuum and argon, respectively. (d) Galvanostatic curves for a Li/electrodeposited Ni film cell. The deposit was heated at 500 °C under argon.

the same set of peaks as that for the undischarged film shown in Fig. 1c. This characteristic, and the lack of peaks for nickel and lithium phosphide, question the assignation of the capacity delivered by the cell to reaction (2). As stated above, the surface of this film is coated with a layer of oxide –Fe_2O_3 as identified by XRD– of significant thickness (more than one hundred nanometers). Transition metal oxides are known to react reversibly with lithium according to the following model:

$$M_xO_y + 2yLi \leftrightarrow xM + yLi_2O(M = Ni, Fe) \quad (3)$$

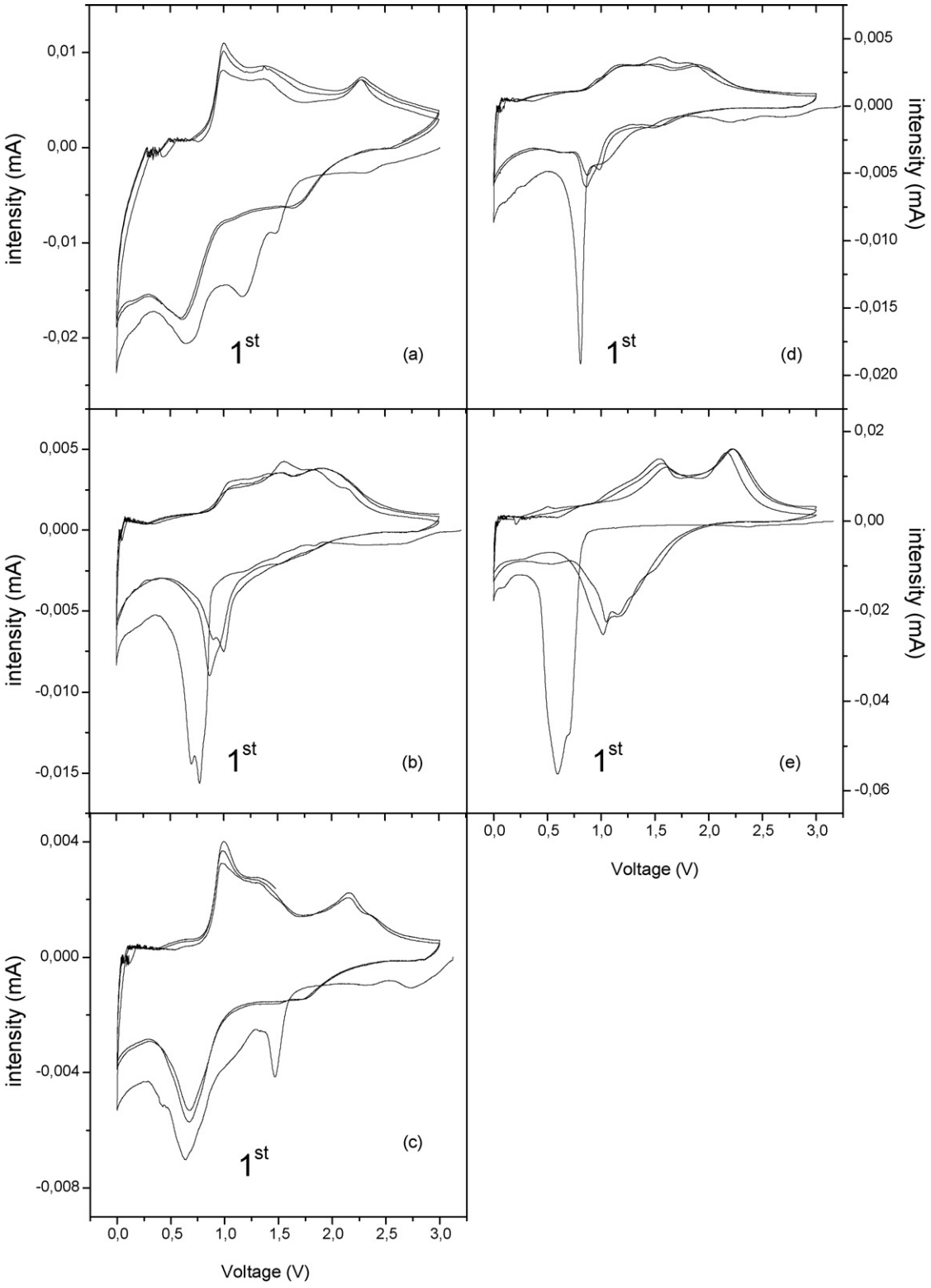

Fig. 5. SPES curves for Li/electrodeposited Ni–P film cells: (a) pristine film, (b) film heated under argon and (c) film heated under vacuum. (d) Curves for the Li/substrate cell. (e) Curves for the Li/electrodeposited Ni film. This film was heated under argon.

Moreover, the discharge curves for M_xO_y/Li cells resemble those of Fig. 4c [26]. The shape of the second discharge curve is also different from those for the other two films, the main difference being the presence of a short plateau close to 1.2 V.

The SPES curves provide more accurate information with a view to identifying the electrochemical reactions undergone by the films and are more appropriate for establishing similarities and differences in electrochemical behaviour between the electrodes. For easier understanding, we will first describe the films exhibiting the strongest differences in the galvanostatic curves, namely: the pristine film and that heated under argon. Fig. 5a and b show the first three potentiostatic curves for the electrodes made from these films. The shape and position of the peaks in the cathodic and anodic scan are clearly different. Thus, the strong peak at 0.5 V for the heated film in the first discharge, Fig. 5b, shifts to lower values and shrinks significantly in the second discharge. The shape of the first charge curve clearly differs from that of the discharge curve, the most marked difference being the absence of a peak accounting for the reversibility of the main reaction giving the strong peak observed in the cathodic scan. This peak may be mainly due to electrolyte decomposition catalysed by the oxide layer. The SPES curves for the pristine film, Fig. 5a, are more similar; thus, the main peak in the discharge curve at 0.6 V has its counterpart shifted to somewhat higher potentials (*ca.* 1 V) in the charge curve. On further cycling, the curves maintained their same shape except for the peak at 1.2 V in the first discharge, which was absent and the origin of which may be the reduction of the thin contamination layer as revealed from XPS depth profile analysis (Fig. 3). Thus, the electrochemical reaction undergone by the pristine film is reversible and, as shown by XRD and XPS, must involve the amorphous phosphide as in reaction (1) and/or (2). Fig. 5c shows the SPES curves for electrode made from the film heated in vacuum. As expected, the shape and position of the peaks are quite similar to those of pristine film, except for the first discharge curve. Nevertheless, for this curve, the main difference affects to the peaks intensity but not to their position.

Two additional measurements confirmed the significant role played by the transition metal oxide layer on the electrochemical properties of the film heated under Ar. The uncoated substrate (stainless steel) and electrodeposited Ni heated under argon were used as electrodes in lithium cells. Nickel is known to be inert against lithium, prepared as nanosized grains; however, electrolyte can be reduced onto nickel foil [27] and nanosized materials can promote this effect [28]. The XPS data for these electrodes (results not shown) also revealed the presence of oxygen strongly bound to the surface. The SPES curves are shown in Fig. 5d and e. The results of these two measurements share some features and are comparable to those of Fig. 5b as regards (i) the presence of a strong peak at 0.8–0.6 V the first discharge curve that disappears in the second discharge and is replaced by weaker peaks at somewhat higher voltages; and (ii) the absence of a strong, equivalent peak in the charge curves, which indicates that the reaction giving the strong reduction peak is irreversible. These results are consistent with the galvanostatic curves, where a clear similarity was observed between the electrodes made from Ni–P and Ni films heated under argon (Fig. 4c and d,

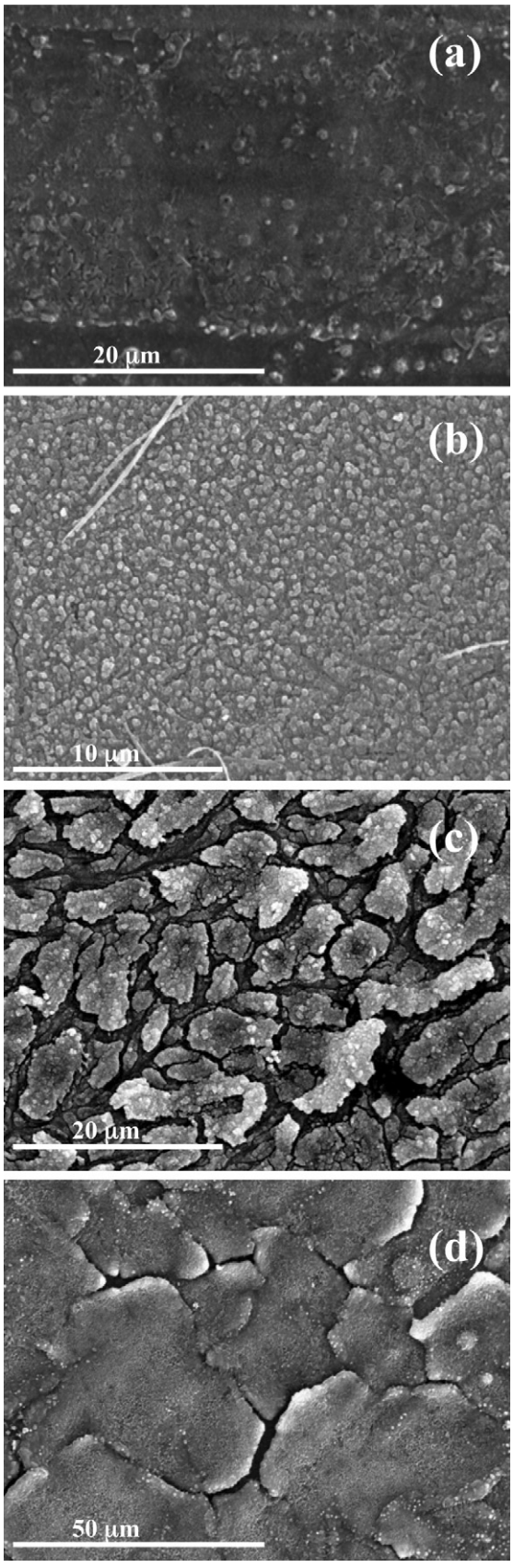

Fig. 6. SEM images for the films after cycling: (a) pristine film, (b and c) film heated under vacuum or argon, respectively; (d) electrodeposited Ni film heated under argon.

respectively). We interpret this similarity by assuming that the cells essentially involve the same reaction, *viz.* the electrolyte decomposition on the oxidized surface of the electrodes, which is facilitated by the porosity and roughness of the surface [29]. The result is the formation of a thick solid state interface (SEI) that hinders reactions (1) and (2).

3.3. Examination of the electrodes after the electrochemical reaction

As stated above, the XRD data for the discharged Ni_3P electrodes revealed differences in reactivity between the films heated under argon and vacuum (Fig. 1d). The main difference was the presence of peaks for the latter film associated to new phases, namely well crystallized LiP (JCPDS 42-790) and nickel of low crystallinity. The presence of these phases is consistent with reaction (1); however, the peaks assigned to the pristine phase reveals that the reaction only affects the deposit to a certain depth, the thickness of which is unknown. By contrast, the XRD pattern for the film heated under argon is consistent with a low Ni_3P reactivity and with the reduction involving both the electrolyte and the iron oxide. In fact, this film possesses an iron oxide layer of greater thickness as revealed by the XPS depth profiles (Fig. 3) and clearly detected by XRD (Fig. 1c). The surface morphology of the electrode after cycling was also influenced by the heating conditions. The pristine film and that heated under vacuum, (Fig. 6a and b) exhibited little cracking at the surface. By contrast, the film obtained under argon (Fig. 6c) exhibited a severely fragmented surface and the deposit resembles an archipelago of islands of uneven size. The image was quite similar to that of the discharged nickel film electrode (Fig. 6d). Therefore, the electrochemical process strongly degrades the surface of the latter two films.

The XPS data for the discharged electrodes are consistent with the previous results. Accurately determining the element contents was made impossible by the presence of electrolyte residues on the surface. For this reason, the discussion is focussed on Ni as it was the main component of the film and its peaks were reasonably well resolved. The Ni $2p_{3/2}$ emission peak is shown in Fig. 7. After sputtering for a few minutes, the spectrum for the film heated under argon was similar to that recorded prior to the discharge measurement (Fig. 7a); this is consistent with the low reactivity of the film towards lithium. By contrast, the Ni $2p_{3/2}$ signal for the film heated under vacuum was different and consisted of two components (Fig. 7b). The low energy, weaker peak, coincides with that for the argon heated electrode and suggests the presence of unreacted Ni–P alloy. On the other hand, the high energy, stronger peak, can be assigned to Ni–O species most probably formed by rapid oxidation of nickel nanoparticles produced by reactions (1) or (2).

3.4. Cycling properties of the films

We examined the cycling properties of the pristine film and that heated in vacuum, the combination of structural and electrochemical data for which suggested a certain reactivity of the Ni–P alloy towards lithium. Fig. 8 shows the capacity delivered by the cells, referred to the total mass of the film, as a function of number of cycles. Cells were cycled over the range 2.0–0.0 V under C/10. The two electrodes exhibit some similarities that are worth some comment. Thus, the decrease from the first discharge to the second was nearly identical and has been discussed previously. The following cycles exposed no regular trend. Thus, the capacity increased between the 10th and 20th cycle; on further cycling, however, the tendency was to a slow decrease. The average capacity delivered by the amorphous electrode over

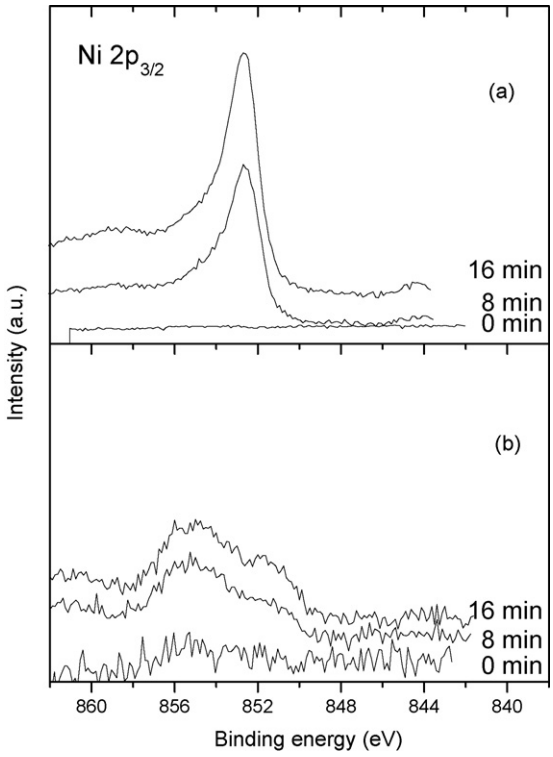

Fig. 7. XPS Ni $2p_{3/2}$ emission peak for Ni–P electrodeposited film heated under argon (a) or vacuum (b). Sputtering times are indicated next to the curve.

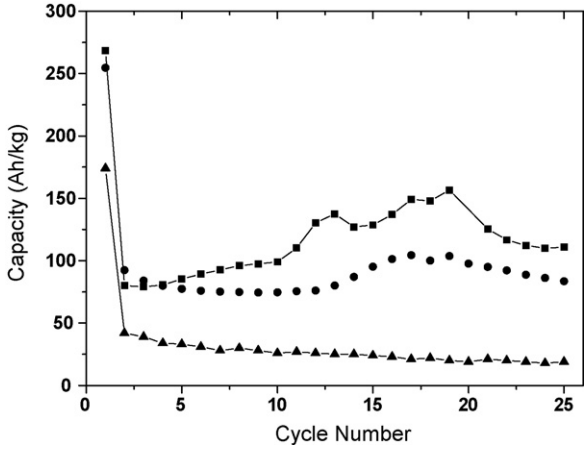

Fig. 8. Cycling properties of the cells based on (■) Ni–P pristine film, (●) Ni–P film heated under vacuum. (▲) Cell based on bulk crystalline Ni_3P.

the 25 cycles studied (*ca.* 115 A h kg^{-1}) was higher than that calculated for the heated electrode (*ca.* 85 A h kg^{-1}); also, it is similar to that calculated from reaction (1) (126 A h kg^{-1} at $x = 0$), but markedly lower from that for the complete reaction (2) (388 A h kg^{-1} at $y = 0$). Expanding the voltage window up to 3.0 V should facilitate SEI dissolution [1], thereby reducing the electrode impedance and increasing the reversibility of the reaction. However, it would be detrimental with a view to using the alloy as anode material for batteries, as it would diminish the potential delivered by the cell. Nevertheless, the capacity retention of these electrodes was better than that for bulk Ni_3P alloy prepared by direct synthesis from its elements (see Fig. 8) even though some carbon black was added to the pellets in order to improve electronic conductivity. In fact, as previously found in other metal phosphides, the reversibility of the reaction between this alloy and lithium is quite limited. Therefore, preparing of the alloy as thin films improves its performance as an electrode material for lithium cells.

4. Conclusions

The electrodeposition technique is an effective method for preparing thin films of amorphous nickel phosphide that can be converted into crystalline Ni_3P by heating. We explored two heating atmospheres and their influence on the morphology, composition and electrochemical properties of the films. XPS analyses revealed that the thermally treated films are coated by an oxide layer that was identified as hematite by XRD in the film heated under argon. This coating layer can be removed by argon etching and its thickness increases in the following sequence: pristine compound < film heated under vacuum < film heated under argon. The surface morphology of the latter film underwent the more significant changes, (an increased porosity of the deposit). Both the composition and surface morphology of the film have a very strong effect on its electrochemical properties in lithium cells. In the film obtained under argon, the presence of a thicker oxide coating and a more porous structure favour two side reactions (*viz.* reaction (3) and electrolyte reduction) at the expense of reactions (1) and (2). These two side reactions are less favourable in the other two types of films (particularly the pristine film), and the average capacity measured over the first 25 cycles is consistent with that calculated from reaction (1).

Acknowledgements

The authors wish to acknowledge funding from Spain's Education and Science Ministry through Project MAT2005-03069. J.S.P. is also grateful to Junta de Andalucía (Spain) for inclusion in the Researcher Return Program.

References

[1] P. Poizot, S. Laruelle, S. Grugeon, L. Dupont, J.M. Tarascon, Nature 407 (2000) 496.
[2] D. Larcher, M. Masquelier, C.D. Bonnin, Y. Chabre, V. Masson, J.B. Leriche, J.M. Tarascon, J. Electrochem. Soc. 150 (2003) A133.
[3] M.N. Obrovac, R.A. Dunlap, R.J. Sanderson, J.R. Dahn, J. Electrochem. Soc. 148 (2001) A576.
[4] Z. Yuan, F. Huang, C. Feng, J. Sun, Y. Zhou, Mater. Chem. Phys. 79 (2003) 1.
[5] J. Morales, L. Sánchez, F. Martín, J.R. Ramos-Barrado, M. Sánchez, Electrochim. Acta 49 (2004) 4589.
[6] J. Morales, L. Sánchez, S. Bijani, L. Martínez, M. Gabás, J.R. Ramos-Barrado, Electrochem. Solid-State Lett. 8 (2005) A159.
[7] H. Li, G. Richter, J. Mater, Adv. Mater. 15 (2003) 736.
[8] N. Pereira, L. Dupont, J.M. Tarascon, L.C. Klein, G.G. Amatucci, J. Electrochem. Soc. 150 (2003) A1273.
[9] F. Guillot, L. Monconduit, M. Morcrette, M.-L. Doublet, L. Dupont, J.M. Tarascon, Chem. Mater. 17 (2005) 3627.
[10] D.C.C. Silva, O. Crosnier, G. Ouvrard, J. Greedan, A. Safa-Sefat, L.F. Nazar, Electrochem. Solid-State Lett. 6 (2003) A162.
[11] V. Pralong, D.C.S. Souza, K.T. Leung, L.F. Nazar, Electrochem. Commun. 4 (2002) 516;
Z. Zhang, J. Yang, Y. Nuli, B. Wang, J. Xu, Solid State Ionics 176 (2005) 693.
[12] H. Pfeiffer, F. Tancret, M.-P. Bichat, L. Monconduit, F. Faiver, T. Brousse, Electrochem. Commun. 6 (2004) 263;
H. Pfeiffer, F. Tancret, T. Brousse, Electrochim. Acta 50 (2005) 4763.
[13] F. Gillot, M.P. Bichat, F. Favier, M. Morcrette, M.L. Doublet, L. Monconduit, Electrochim. Acta 49 (2004) 2325.
[14] K. Wang, J. Yang, J. Xie, B. Wang, Z. Wen, Electrochem. Commun. 5 (2003) 480.
[15] M.-P. Bichat, T. Politova, H. Pfeiffer, F. Tancret, L. Monconduit, J.-L. Pascal, T. Brousse, F. Favier, J. Power Sources 136 (2004) 80.
[16] F. Gillot, S. Boyanov, L. Dupont, M.-L. Doublet, M. Morcrette, L. Monconduit, J.M. Tarascon, Chem. Mater. 17 (2005) 6327.
[17] M.M.V. Parente, O.R. Mattos, S.L. Díaz, P. Lima Neto, F.J. Fabri Miranda, J. Appl. Electrochem. 31 (2001) 677.
[18] J.L. Carbajal, R.E. White, J. Electrochem. Soc. 135 (1988) 2952;
A. Królikowski, P. Butkiewicz, Electrochim. Acta 38 (1993) 1979.
[19] C.S. Lin, C.Y. Lee, F.J. Chen, W.C. Li, J. Electrochem. Soc. 152 (2003) C370;
M. Saitou, Y. Okudaira, W. Oshikawa, J. Electrochem. Soc. 150 (2003) C140.
[20] Modern Electroplating, fouth ed., Morcheday Schlensinger and Milan Paunovic, ed., Wiley Interscience, 2000.
[21] I. Paseka, Electrochim. Acta 47 (2001) 921.
[22] M.C. Oliveira, A.M. Botelho do Rego, J. Alloy Comp. 425 (2006) 64.
[23] S.J. Sawhill, D.C. Phillips, M.E. Bussell, J. Catal. 215 (2003) 208.
[24] R. Franke, Spectrochim. Acta Part A 53 (1997) 933.
[25] J.F. Moulder, W.F. Stickle, P.E. Sool, K.D. Bomber, Handbook of X-ray Photoelectron Spectroscopy, Perkin-Elmer, Eden Praire, 1992.
[26] C. Jiang, E. Hosono, H. Zhon, Nanotoday 1 (2004) 28.
[27] A. Zaban, D. Aurbach, J. Power Sources 54 (1995) 289.
[28] M. Winter, J.O. Besenhard, Electrochim. Acta 45 (1999) 31;
H. Li, L. Shi, Q. Wang, L. Chen, X. Huang, Solid State Ionics 148 (2002) 247.
[29] S. Grugeon, S. Laruelle, L. Dupont, F. Chevallier, P.L. Taberna, P. Simon, L. Gireaud, S. Lascaud, E. Vidal, B. Yrieux, J.M. Tarascon, Chem. Mater. 17 (2005) 5041.